Light nuclei production in heavy-ion collisions at relativistic energies

S. Albergo,[4] R. Bellwied,[11] M. Bennett,[9] B. Bonner,[7] H. Caines,[7] W. Christie,[1] S. Costa,[4] H. J. Crawford,[9] M. Cronqvist,[9] R. Debbe,[1] J. Engelage,[9] L. Greiner,[9] T. Hallman,[1] G. Hijazi,[11] G. Hoffmann,[10] H. Z. Huang,[2] T. J. Humanic,[7] A. Insolia,[4] P. Jensen,[10] E. G. Judd,[9] K. Kainz,[8] M. Kaplan,[3] S. Kelly,[2] I. Kotov,[7] G. Kunde,[12] P. J. Lindstrom,[5] W. Llope,[8] G. LoCurto,[7] R. Longacre,[1] D. Lynn,[1] N. Mahzeh,[11] Z. Milosevich,[3] J. T. Mitchell,[1] J. W. Mitchell,[6] S. Nehmeh,[11] S. Paganis,[10] S. U. Pandey,[11] R. Potenza,[4] D. E. Russ,[3] A. Saulys,[1] J. Schambach,[10] J. Sheen,[11] E. Sugarbaker,[7] J. Takahashi,[1] J. Tang,[10] A. L. Trattner,[9] S. Trentalange,[2] A. Tricomi,[4] C. Tuvè,[4] J. P. Whitfield,[3] and K. Wilson[11]

[1]*Brookhaven National Laboratory, Upton, New York*
[2]*University of California, Los Angeles, California*
[3]*Carnegie Mellon University, Pittsburgh, Pennsylvania*
[4]*Università di Catania and INFN, Sezione di Catania, Catania, Italy*
[5]*Lawrence Berkeley National Laboratory, Berkeley, California*
[6]*NASA Goddard Space Flight Center, Greenbelt, Maryland*
[7]*The Ohio State University, Columbus, Ohio*
[8]*Rice University, Houston, Texas*
[9]*Space Science Laboratories, University of California, Berkeley, California*
[10]*University of Texas, Austin, Texas*
[11]*Wayne State University, Detroit, Michigan*
[12]*Yale University, New Haven, Connecticut*

(Received 24 August 2001; published 4 March 2002)

We have measured the production of light nuclei ($A \leqslant 3$) in 11.6 GeV/c Au-Au collisions at the Brookhaven Alternating Gradient Synchrotron (AGS). The transverse mass spectra are analyzed using a thermal fireball model, and the yields for different particle species are discussed assuming coalescence and fragmentation as possible production mechanisms. The wide acceptance range of the ^{3}He measurements permits a broad study of the coalescence parameter B_3 as functions of transverse momentum and rapidity. Comparisons with data obtained previously at AGS energies suggest that the simple models are insufficient to describe fully the production mechanisms of light nuclei.

DOI: 10.1103/PhysRevC.65.034907 PACS number(s): 25.75.−q

I. INTRODUCTION

The study of light nuclei production in heavy-ion collisions provides an interesting tool for understanding the reaction dynamics based on the phase space dependencies of different production mechanisms. At AGS energies, it is very unlikely that light nuclei ($A \geqslant 2$) are produced via direct hadronization. The available energy of 3.1 GeV in each nucleon-nucleon collision at 11.6 GeV/c is slightly below the deuteron production threshold of 3.7 GeV. Therefore only additional contributions from collective or Fermi motion will enable the direct production. Thus the majority of the measured light nuclei are either beam and target fragments, or they are produced via coalescence of nucleons in the fireball. If fragments survive the rather violent collisions at these energies, one would expect them to be observed only near beam and target rapidities, whereas production through coalescence would dominate the central rapidity region.

The coalescence model was initially developed for deuteron production considering phase-space probability distributions of the proton and neutron [1–4]. In this model, the protons and neutrons interact via the strong force coupled to a third body which allows them to bind and form the deuteron. Considering only the momentum phase space, the deuteron probability density is thus proportional to the density of protons and neutrons. In heavy-ion collisions, the neutron momentum distribution is similar to the proton momentum distribution [5–8]. Thus, extending the phase-space relation to heavier clusters, the density in momentum phase space of a cluster of mass A can be expressed as

$$E_A \frac{d^3N_A}{d^3p_A} = B_A \left(E_p \frac{d^3N_{protons}}{d^3p_{protons}} \right)^A, \tag{1}$$

where B_A corresponds to the coalescence probability

$$B_A = \left(\frac{2s_A+1}{2^A} \right) \frac{1}{N!Z!} (R_{np})^N \left(\frac{4\pi}{3} p_0^3 \right)^{A-1}. \tag{2}$$

N and Z are the neutron and proton number of the composite particle, s_A is the spin of the particle, R_{np} is a scale factor that accounts for the isospin distribution of the colliding nuclei, and p_0 is the maximum relative momentum at which the nucleons will coalesce. In this formulation, the coalescence factor B_A is unique for each particle species but does not vary with beam energy and, except for small variations of R_{np}, it is also independent of the colliding system.

II. EXPERIMENT

AGS experiment 896 was a heavy-ion fixed target experiment measuring ^{197}Au+^{197}Au collisions with a beam momentum of 11.6 GeV/c per nucleon. The experiment was performed at the Alternating Gradient Synchrotron accelera-

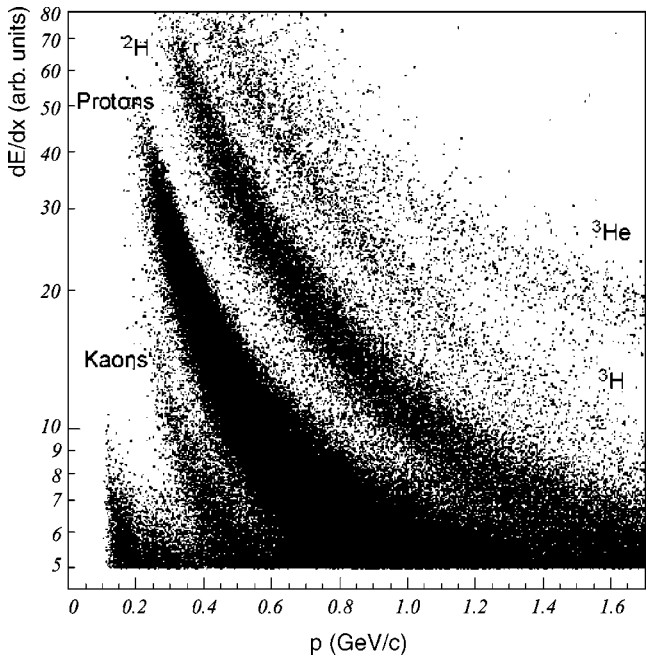

FIG. 1. dE/dx plot as a function of particle momentum.

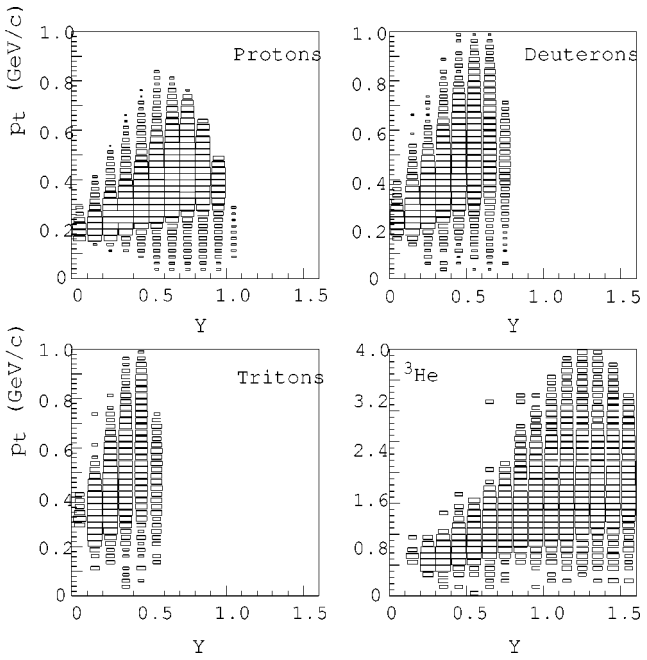

FIG. 2. Measured range of p_t versus rapidity of the identified particles: protons, deuterons, tritons, and ^{3}He.

tor (AGS) at Brookhaven National Laboratory. The main physics motivation for this experiment was the search for the H_0 dibaryon [9], an exotic six-quark state which has never been unambiguously observed.

An array of 15 silicon drift detectors (SDDA) was used for charged particle tracking. It was positioned inside a 6.2-T magnetic field at a closest distance of 8 cm from the gold target. Due to its proximity to the target, the detector had excellent solid angle coverage for primary particles and a high sensitivity for short-lived particles such as Λ's [10]. A detailed experimental description is presented elsewhere [11–13].

A total of 350 000 central Au+Au events were analyzed with the silicon detector array. Centrality is defined by a measurement of the particle multiplicity in each event. This measurement was performed with an array of scintillators covering a pseudorapidity range between $\eta=1.9$ and 3.3. For all events recorded with E896 a cut on the multiplicity was applied which corresponds to the upper 5% of the geometrical cross section. Track reconstruction was performed requiring a minimum of 5 hits on each track in order to minimize the number of ghost tracks and improve momentum resolution. On average, 50 tracks per event were reconstructed in the silicon detector array. Particle identification was accomplished by measuring the energy loss (dE/dx) of each charged particle in each silicon plane. The average energy loss of a particle track, dE/dx, was then determined using a truncated mean of the lower 75% of all detector plane measurements. Figure 1 shows the extracted energy loss as a function of particle momentum. To separate the different particles, the distributions were divided into momentum intervals of 0.1 GeV/c, projected onto the dE/dx axis, and fitted with Landau distributions for each particle. In each projection, the overlap areas between the fit curves corresponding to different particles were used to determine the contamination factors for each particle yield.

Figure 2 shows the measured range of the identified particles in transverse momentum versus rapidity. The acceptance here is constrained by the detector solid angle and the dE/dx interval in which it is possible to identify the particle. Acceptance correction factors were calculated by propagating Monte Carlo generated events through GEANT [14]. The simulated GEANT tracks were then embedded into real events to calculate the track reconstruction efficiency. Since the tracking efficiency varies with hit density a single GEANT track was embedded in each event. Detector position and double track resolution were also considered in the embedding procedure. On average, the track reconstruction efficiency for primary particles was around 90%. Acceptance and efficiency corrections were calculated and applied separately for each y-p_t bin for each particle species.

III. RESULTS

Figures 3–6 show the invariant yields per collision of protons, deuterons, tritons (^{3}H) and helium (^{3}He) as a function of the transverse mass, m_t-m_0, for various rapidity bins. In these plots, measurement errors include the statistical uncertainty coupled to the uncertainty introduced by contamination factors in the particle identification. Systematic errors due to the resolution in the transverse momentum are not included in the error bars plotted in Figs. 3–6; however, they were considered in the fit procedure and they account for less than 10% of the total uncertainty in the fit range.

The invariant double differential spectra are fitted with the Boltzmann curve according to a thermal fireball model [15,16]:

$$\frac{1}{2\pi m_t}\frac{d^2N}{dy\,dm_t}=C(y)m_t e^{(-m_t/T)}, \tag{3}$$

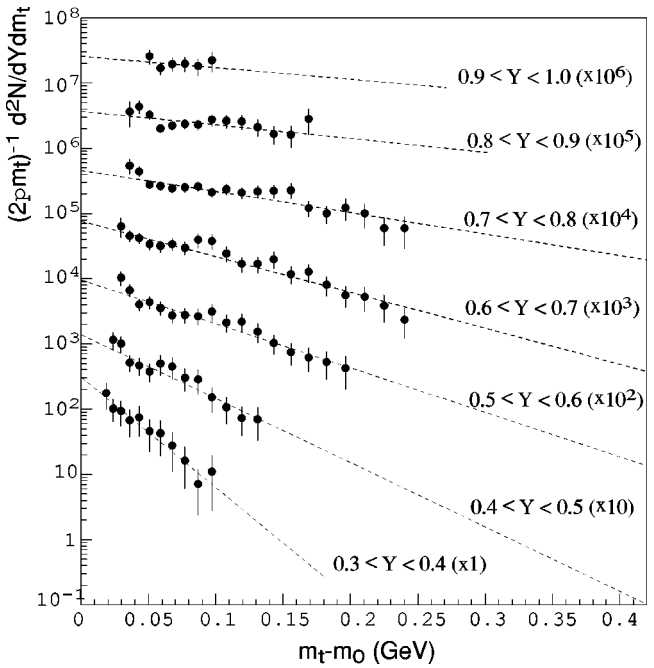

FIG. 3. Measured double differential yields of protons for different rapidity intervals as a function of transverse mass $m_t - m_0$. The dashed lines represent fits to Eq. (3).

where $C(y)$ and T (inverse slope) were the free parameters of the fit. Fit results of inverse slope parameters for E896 protons, deuterons, and ^{3}He are shown in Fig. 7 as a function of y/y_{beam}. For comparison, midrapidity protons from experiment E866 [17] (Au+Au at 11.6A GeV/c) are also plotted in Fig. 7.

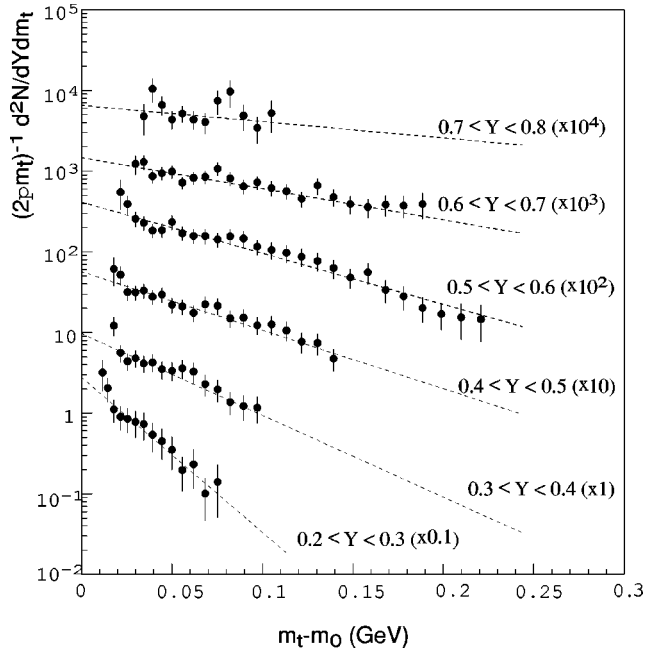

FIG. 4. Measured double differential yields of deuterons for different rapidity intervals as a function of transverse mass $m_t - m_0$. The dashed lines represent fits to Eq. (3).

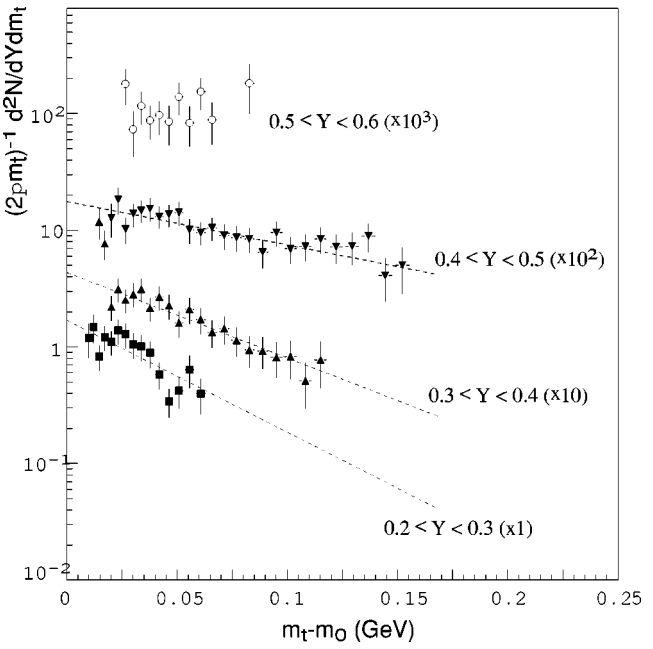

FIG. 5. Measured double differential yields of tritons for different rapidity intervals as a function of transverse mass $m_t - m_0$. The dashed lines represent fits to Eq. (3).

According to most thermal model calculations the midrapidity slope parameters correspond to the freeze-out temperature, which should be the same for the different particle species emitted from the fireball. However, if one considers transverse expansion [18] of the source before freeze-out, then the effective slope parameter for each particle can be parametrized as the sum of the freeze-out temperature and a

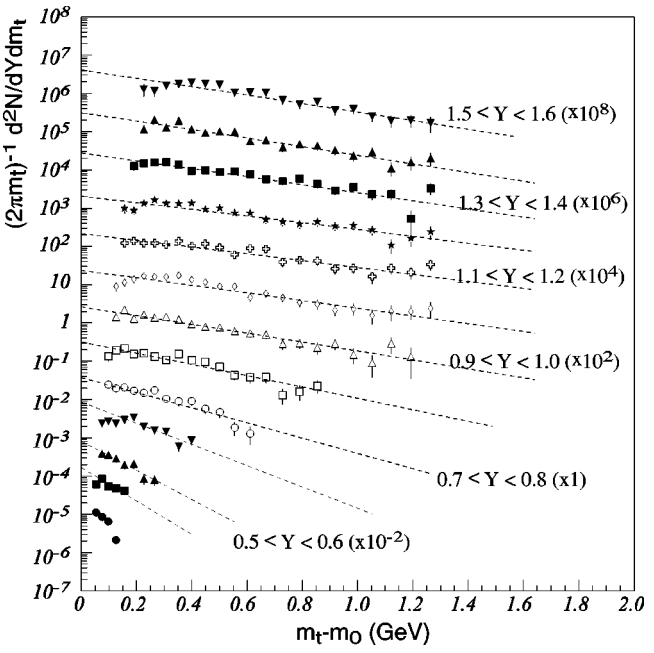

FIG. 6. Measured double differential yields of ^{3}He isotope for different rapidity intervals as a function of transverse mass $m_t - m_0$. The dashed lines represent fits to Eq. (3).

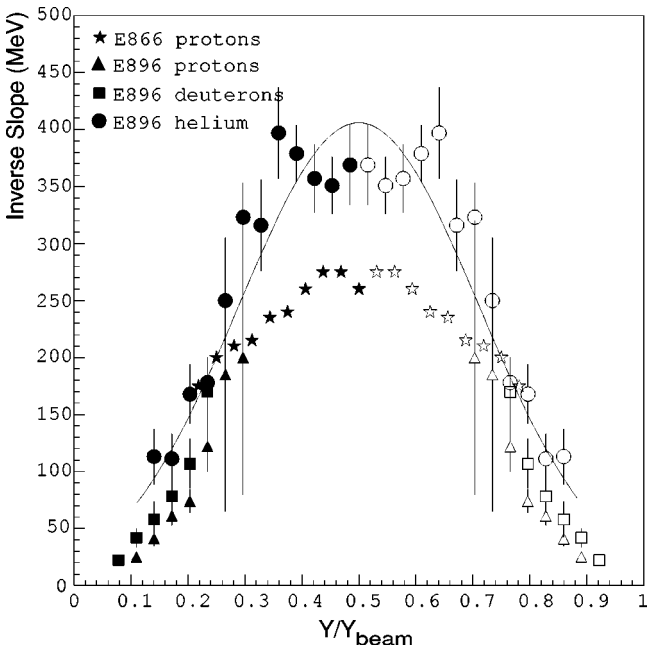

FIG. 7. Slope parameters as a function of rapidity for protons from E866 (stars) in comparison to E896 protons (triangles), deuterons (squares), and ^{3}He (circles). The solid symbols represent the measured data and the corresponding open symbols represent the data reflected symmetrically around midrapidity ($y=1.6$).

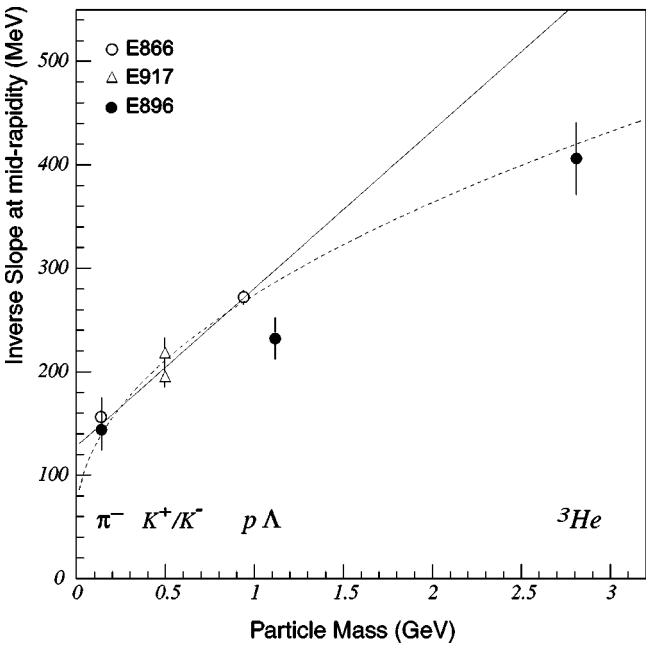

FIG. 8. Compilation of slope parameters at midrapidity for different particle species. π, Λ, and ^{3}He were measured by E896 (solid circles) compared to pions and protons from E866 (open circles) and kaons from E917 (open triangles). The solid line was calculated presuming a linear dependence, generated by a box profile of the source density and the dashed line represents the adjusted curve assuming a $\sqrt{A}$ dependence generated by a Gaussian profile of the source density.

term that is proportional to the square of the source average transverse expansion velocity $\langle\beta_t\rangle^2$ scaled by a coefficient D which is a function of the particle mass A,

$$T_{eff}=T_{freeze\text{-}out}+D(A)\cdot\langle\beta_t\rangle^2. \tag{4}$$

Figure 8 shows a compilation of inverse slope parameters as a function of particle mass for midrapidity particles measured in 11.6 GeV/c Au+Au reactions. The pion, lambda, and ^{3}He slope parameters are calculated from this experiments data. The E896 lambda analysis and the deviation of the lambda inverse slope from the general mass dependence are discussed in a separate paper [10]. Proton and kaon slope parameters are extracted from AGS experiment E866 and E917 [19], respectively. Particle species with mass below the proton mass fall on a common linear curve [$D(A)=A$] that yields a common freeze-out temperature of 128 ± 15 MeV and an average transverse expansion velocity of $\langle\beta_t\rangle=0.39\pm0.14$ according to Eq. (4).

The ^{3}He inverse slope parameter at mid-rapidity yields a lower value as compared to the linear systematic. In a recent paper by Polleri *et al.* [20] the coefficient $D(A)$ for light nuclei was calculated analytically considering two different profiles for the nucleon density in the fireball. In the case of a Gaussian density profile the coefficient is proportional to $\sqrt{A}$, whereas a constant (box-shaped) density profile yields a coefficient proportional to A. Both extrapolations are shown in Fig. 8 and the Gaussian profile fit is in better agreement with the data.

The total cross section for each rapidity bin is calculated by integrating the respective m_t spectra over the full phase space range:

$$\frac{dN}{dy}=\int_{m_0}^{\infty}2\pi m_t\frac{d^2N}{2\pi m_t dy dm_t}dm_t. \tag{5}$$

This integral is less sensitive to the fit range than the slope parameters; thus the fits shown in Figs. 3 –6 (including the protons and tritons) were used to extrapolate the integrated dN/dy for each rapidity bin. Figure 9 shows the dN/dy distributions for the different particles. Error bars were calculated by propagating the uncertainties of the fit parameters using Eq. (5).

The proton production is well measured by various AGS experiments and is reliably reproduced by existing models. The RQMD V2.4 [21] prediction for protons produced in 11.6 GeV/c central Au+Au collisions is plotted as a dashed line in Fig. 9. It shows good agreement with the data within the measurement errors. Also plotted, using open circles and triangles, are the yields of protons and deuterons measured by experiment E866 [17] for the same reaction. E866 did only consider statistical errors in their results. In the overlap region, both experimental data sets show good agreement, when taking into account a moderate systematic error in the E866 measurement.

For all shown particle species there seems to be a change in the dN/dy distribution below $y/y_{beam}=0.3$. The apparent rise in yield could be attributed to a change in production mechanism from coalescence at midrapidity to target fragmentation at the very backward rapidities. E896 uniquely measures this transition region, in particular for the $A=3$ particles (^{3}He).

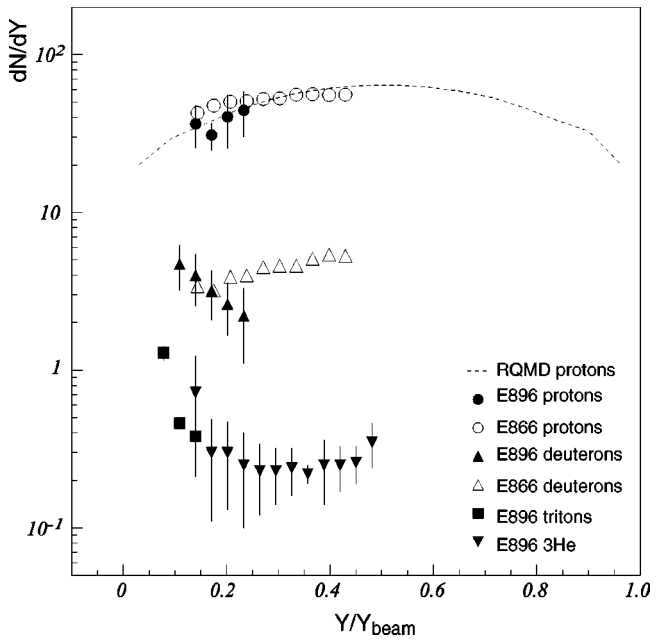

FIG. 9. dN/dy distribution as a function of rapidity for protons, deuterons, tritons, and ^{3}He. The dashed line represents the RQMD prediction for protons. Open symbols represent similar measurements of protons and deuterons presented by AGS experiment 866. Error bars reflect the fits shown in Figs. 3–6.

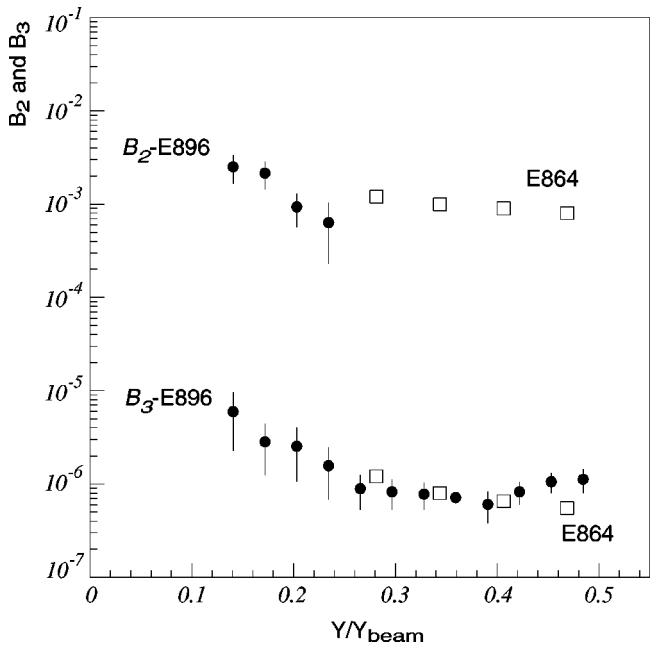

FIG. 10. Coalescence parameters calculated through yield ratios d/p^2 for B_2 and t/p^3 and ^{3}He/p^3 for B_3 as a function of rapidity for $p_t<100$ MeV (solid symbols). B_2 and B_3 results measured by AGS experiment 864 are presented in open squares.

Another indicator of such a behavior is shown in the comparison of coalescence factors for midrapidity and backward rapidity. Based on Eq. (1), the coalescence factors B_2 and B_3 were calculated through the ratios d/p^2 and ^{3}He/p^3, respectively, for each rapidity interval as a function of p_t. Since the detector acceptance for protons is limited, and we have shown in Fig. 9 that RQMD describes the proton data well within the measured range, the coalescence parameters were calculated by fitting the measured yields of the deuterons and ^{3}He and dividing these fit functions by the appropriate power of the proton yield as predicted by RQMD. Figure 10 summarizes the coalescence factors obtained as a function of rapidity for a particular low p_t interval ($p_t<100$ MeV/c). For comparison, the B_2 and B_3 parameters measured by experiment E864 [23] are also plotted (open squares).

In the mid-rapidity region ($y/y_{beam}>0.3$), both parameters remain approximately constant, as expected from the coalescence model. However, in the backward rapidity range ($y/y_{beam}<0.3$), the coalescence factor varies with rapidity, again suggesting that a different production mechanism, most likely fragmentation, might contribute to the particle yields in addition to the yield expected from simple coalescence.

Figure 11 corroborates the rapidity dependence of the particle production by comparing coalescence penalty factors as a function of particle mass for the two different rapidity regions. This factor is an empirical quantity, which parametrizes the particle yield as a function of particle mass assuming that each additional nucleon in the coalescence process will cause a decrease in yield [22]. Here, the integrated cross sections for light nuclei particles at mid-rapidity measured by experiment E864 ($y/y_{beam}=0.6$) [23], are compared to the integrated cross sections obtained in E896 at backward rapidity ($y/y_{beam}=0.2$). In both analyses the same p_t intervals were used. The power law parametrization is a good description for the particle yields in both cases. The numerator determines the intercept, whereas the denominator shows the actual penalty factor per nucleon. The comparison shows that in the lower rapidity range the penalty factor for

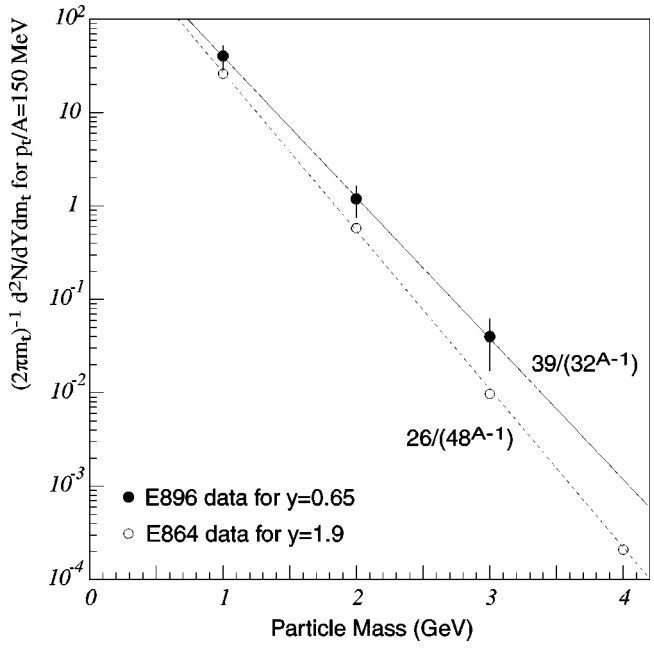

FIG. 11. Mass dependence of the invariant yields of light nuclei. Yields measured for p_t/A between 100 and 200 MeV at $y/y_{beam}=0.2$ from E896 and $y/y_{beam}=0.6$ from E864.

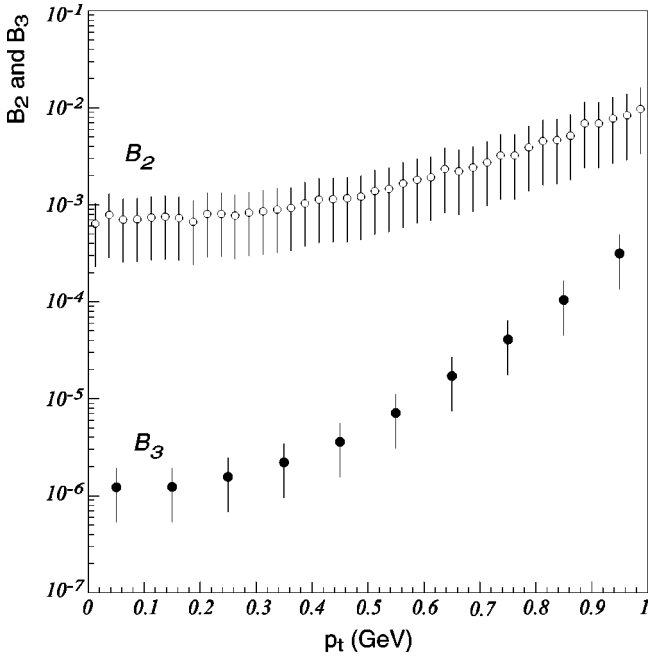

FIG. 12. Coalescence factors B_2 (open circles) and B_3 (solid circles) calculated by the yield ratios d/p^2 and $^3\mathrm{He}/p^3$ as a function of p_t for the rapidity interval $0.22<y/y_{beam}<0.25$.

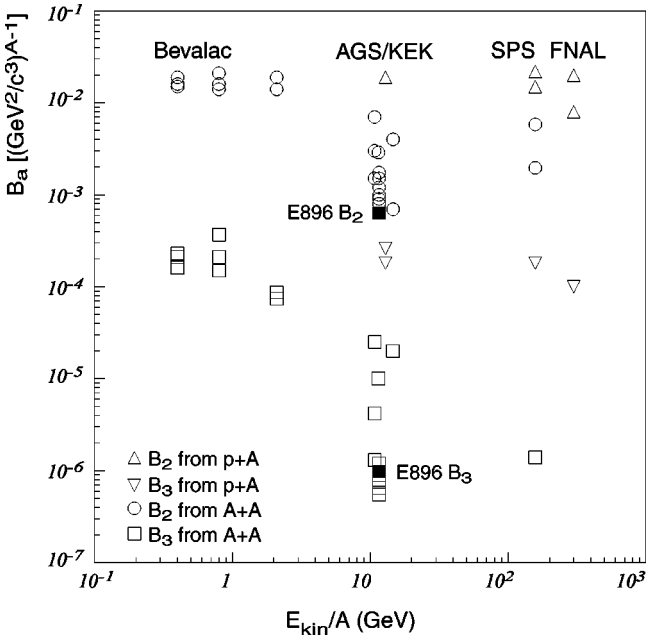

FIG. 13. Compilation of coalescence parameters B_2 (circles) and B_3 (squares) measured in AA collisions at different reaction energies. The triangles (up for B_2, down for B_3) represent measurements in $p+A$ reactions at various incident energies. E896 data points are represented by the solid symbols, representing B_2 and B_3 calculated for the most central rapidity bin and $p_t<1$ GeV/c.

light nuclei production is about 30% lower (32 as opposed to 48) than near mid-rapidity.

Figure 12 shows the coalescence parameters B_2 (open circles) and B_3 (solid circles) as a function of transverse momenta calculated for the rapidity interval $0.22<y/y_{beam}<0.25$. The strong p_t dependence agrees qualitatively with predictions based on a coalescence model that includes collective flow and a constant nucleon density profile [20].

Figure 13 shows a compilation of coalescence parameters B_2 and B_3 as a function of projectile kinetic energy per nucleon (E_{kin}/A) measured by different experiments. The direct comparison of coalescence results from different experiments is difficult since B_A varies with p_t and rapidity (as shown in Figs. 10 and 12). In addition the EOS Collaboration has shown that the system size and collision centrality also impact the light nuclei production [24,25]. However, the comparison in Fig. 13 is meant to show a more general trend of the coalescence probability as a function of beam energy for $p+A$ and $A+A$ reactions. The lower energy results are from Ne+Pb reactions measured at the BEVALAC [26]. The E896 B_2 and B_3 parameters are plotted in Fig. 13 with solid symbols and represent the coalescence parameters calculated for the midrapidity range and $p_t=0$. In addition, measurements from AGS experiments E866 [17], E864 [23], E814 [27], E878 [28], and the CERN experiment NA44 [29] are also plotted. Represented by triangles are the coalescence parameters B_2 and B_3 for $p+A$ reactions measured at KEK [30], CERN SPS [31], and FNAL [32].

The B_A factors calculated for the lower energies agree very well with the simple coalescence model, which predicts these factors to be independent of the beam energy and the colliding system. In $p+A$ collisions this assumption seems to hold also for higher energies. However, the $A+A$ results taken at AGS and SPS energies show a clear deviation from this model by yielding lower coalescence factors in addition to a rather strong energy dependence. The hindrance of the light nuclei production could be attributed to the large volume size of the fireball formed in $A+A$ collision, which is supported by the fact that in $p+A$ reactions, where the fireball is small, the coalescence is still in agreement with the model predictions. Thus spatial separations between the nucleons and the collision dynamics seems to play an important role in the coalescence mechanism.

Considering the dynamics of the coalescence mechanism within a large fireball, it has been suggested [33] that the ratio of deuterons to protons (d/p) is established during the early stages of the reaction. After formation in the fireball the weakly bound deuteron will constantly break up and reform, and if the collisions are frequent enough, the density of deuterons will reach an equilibrium. Since this equilibrium will be governed by the collision frequency, which is dependent on the nucleon density in phase space, the ratio of deuterons to protons will be proportional to the entropy per nucleon in the fireball,

$$S_N = 3.945 - \ln\left(\frac{d}{p}\right). \tag{6}$$

Our analysis yields $S_N \approx 7.0$ for the rapidity bin $y=0.75$, which is in qualitative agreement with the value obtained by E814 [27] ($S_N=12.8$) when taking into account the entropy contribution by the pions. The only SPS experiment to report the entropy per baryon was NA44 [29] which quoted a larger value than the AGS experiments at midrapidity, whereas the

BEVALAC results yielded lower values [34]. The steady increase with incident energy is expected. The question remains whether the large values obtained at SPS energies are consistent with a quark phase.

IV. CONCLUSION

Invariant yields of protons, deuterons, tritons, and ^{3}He were measured and analyzed in the framework of a thermal model. The shape of the rapidity distributions indicate that for light nuclei there are different production mechanisms for different kinematic regions, fragmentation at low rapidities ($y/y_{beam}<0.3$) and coalescence at midrapidity ($y/y_{beam}>0.3$). The dependence of the slope parameters deduced from the invariant spectra at midrapidity as a function of mass A agrees with the model of an expanding fireball with a Gaussian nucleon density profile.

The analysis of the light nuclei production in a coalescence model yields the coalescence factors B_2 and B_3. In the midrapidity range, these factors are approximately constant, as expected in the simple coalescence model. At target rapidities, however, the factors deviate from the model. The increase in B_2 and B_3 at lower rapidities can again be attributed to a change in the production mechanism from a coalescence to a fragmentation process. The p_t dependence of the coalescence parameter is well described assuming a constant nucleon density profile in the expanding source. The discrepancy between this result and the behavior of the slope parameters indicates that the simple coalescence formalism inside an expanding fireball may not be sufficient to fully describe the production of light nuclei in $A+A$ collisions.

ACKNOWLEDGMENTS

We wish to thank the AGS Operations group of the Brookhaven National Laboratory for their support in performing this experiment. This work was supported by the Division of Nuclear Physics of the Office of Science of the U.S. Department of Energy, the U.S. National Science Foundation, and the Brazilian FAPESP-Fundação de Amparo à pesquisa do estado de São Paulo.

[1] J.L. Nagle *et al.*, Phys. Rev. C **53**, 367 (1996).
[2] R. Mattiello *et al.*, Phys. Rev. C **55**, 1443 (1997).
[3] S.T. Butler and C.A. Pearson, Phys. Rev. **129**, 836 (1963).
[4] A. Schwarzschild and C. Zupancic, Phys. Rev. **129**, 854 (1963).
[5] A.S. Goldhaber *et al.*, Phys. Lett. **53B**, 306 (1973).
[6] J. Barrette *et al.*, Phys. Rev. Lett. **64**, 1219 (1990).
[7] J. Barrette *et al.*, Phys. Rev. C **45**, 819 (1992).
[8] T.A. Armstrong *et al.*, Phys. Rev. C **60**, 064903 (1999).
[9] R.L. Jaffe, Phys. Rev. Lett. **38**, 195 (1977).
[10] S. Albergo *et al.* (unpublished).
[11] H. Crawford and the E896 Collaboration, Proposal 896 for the BNL-AGS, "Search for a short-lived H0 dibaryon, short-lived strange matter, and to investigate hyperon production in 11.6 GeV/c/N Au+Au collisions."
[12] W. J. Llope for the E896 Collaboration, *The BNL-AGS Experiment 896*, 12th Winter Workshop on Nuclear Dynamics proceedings, Snowbird, Utah, 1996 (Plenum, New York, 1996).
[13] J. Takahashi *et al.*, Nucl. Instrum. Methods Phys. Res. A **439**, 497 (2000).
[14] R. Brun *et al.*, GEANT 3.12 User's Guide, CERN DATA Handling Division, DD/EE/84-1; GEANT-Detector and Simulation Too, CERN, PM0062, 1993.
[15] H. Dobler *et al.*, Phys. Lett. B **457**, 353 (1999).
[16] J. Barrette *et al.*, Phys. Rev. C **63**, 014902 (2001).
[17] B.B. Back *et al.*, Phys. Rev. Lett. **86**, 1970 (2001); L. Ahle *et al.*, Phys. Rev. C **60**, 064901 (1999).
[18] K. Lee *et al.*, Z. Phys. C **48**, 525 (1990).
[19] L. Ahle *et al.*, Phys. Lett. B **490**, 53 (2000).
[20] A. Polleri *et al.*, Phys. Lett. B **419**, 19 (1998).
[21] H. Sorge *et al.*, Phys. Lett. B **243**, 7 (1990); H. Sorge, Phys. Rev. C **52**, 3291 (1995).
[22] C. Dover *et al.*, Phys. Rev. C **44**, 1636 (1991)
[23] T.A. Armstrong *et al.*, Phys. Rev. Lett. **83**, 5431 (1999); Phys. Rev. C **61**, 064908 (2000).
[24] S. Wang *et al.*, Phys. Rev. Lett. **74**, 2646 (1995).
[25] J.A. Hauger *et al.*, Phys. Rev. C **62**, 024616 (2000).
[26] S. Nagamiya *et al.*, Phys. Rev. C **24**, 971 (1981).
[27] J. Barrette *et al.*, Phys. Rev. C **50**, 1077 (1994).
[28] M.J. Bennett *et al.*, Phys. Rev. C **58**, 1155 (1998).
[29] H. Boggild *et al.*, Nucl. Phys. **A590**, 483c (1995).
[30] N. Saito *et al.*, Phys. Rev. C **49**, 3211 (1994).
[31] M. Bussiere *et al.*, Nucl. Phys. **B174**, 1 (1980).
[32] J.W. Cronin *et al.*, Phys. Rev. D **11**, 3105 (1975).
[33] P.J. Siemens and J.I. Kapusta, Phys. Rev. Lett. **43**, 1486 (1979).
[34] L.P. Csernai and J.I. Kapusta, Phys. Rep. **131**, 223 (1986).